

Cite this: *Dalton Trans.*, 2024, **53**,
4461

Mapping the distribution of electronic states within the 5D_4 and 7F_6 levels of Tb^{3+} complexes with optical spectroscopy†

Nicolaj Kofod, * Margrete Juel Henriksen  and Thomas Just Sørensen *

The $Tb(III)$ ion has the most intense luminescence of the trivalent lanthanide(III) ions. In contrast to $Eu(III)$, where the two levels only include a single state, the high number of electronic states in the ground (7F_6) and emitting (5D_4) levels makes detailed interpretations of the electronic structure—the crystal field—difficult. Here, luminescence emission and excitation spectra of $Tb(III)$ complexes with 1,4,7,10-tetraazacyclododecane-1,4,7,10-tetraacetic acid (DOTA, $[Tb(DOTA)(H_2O)]^-$), ethylenediaminetetraacetic acid (EDTA, $[Tb(EDTA)(H_2O)_3]^-$) and diethylenetriaminepentaacetic acid (DTPA, $[Tb(DTPA)(H_2O)]^{2-}$) as well as the $Tb(III)$ aqua ion ($[Tb(H_2O)_9]^{3+}$) were recorded at room temperature and in frozen solution. Using these data the electronic structure of the 5D_4 multiplets of $Tb(III)$ was mapped by considering the transitions to the singly degenerate 7F_0 state. A detailed spectroscopic investigation was performed and it was found that the 5D_4 multiplet could accurately be described as a single band for $[Tb(H_2O)_9]^{3+}$, $[Tb(DOTA)(H_2O)]^-$ and $[Tb(EDTA)(H_2O)_3]^-$. In contrast, for $[Tb(DTPA)(H_2O)]^{2-}$ two bands were needed. These results demonstrated the ability of describing the electronic structure of the emitting 5D_4 multiplet using emission spectra. This offers an avenue for investigating the relationship between molecular structure and luminescent properties in detailed photophysical studies of $Tb(III)$ ion complexes.

Received 1st November 2023,
Accepted 9th February 2024

DOI: 10.1039/d3dt03657j

rsc.li/dalton

Introduction

Lanthanide luminescence has found widespread use in anti-counterfeiting agents,¹ sensing,^{2,3} bioassays,^{4–7} and display technology.⁸ Terbium(III) ions, in particular, have emerged at the forefront of a number of applications such as FRET-based biosensing,^{9–16} luminescent bioprobes,^{17,18} and single-molecule magnets.^{19–22} In addition, the high energy gap between the emitting 5D_4 level and the lower lying $^7F_{6,0}$ manifold makes $Tb(III)$ luminescence less susceptible to quenching by the chemical environment than other luminescent lanthanides.^{23–25} However, unlike the similarly luminescent $Eu(III)$, extracting useful information about the electronic structure from $Tb(III)$ optical spectra is a difficult task.

In contrast to most other lanthanides, for $Eu(III)$ ions, both the ground state 7F_0 level and main emissive level 5D_0 consist of only a single electronic state. The simplicity of the involved states allows a high level of detail, when investigating the elec-

tronic structure of $Eu(III)$ from the optical spectra alone. The key is that the $Eu(III)$ electronic structure can be obtained from the luminescence spectra because the individual lines—the individual electronic states—can be resolved. Thus, $Eu(III)$ luminescence spectra can be directly linked to the point group symmetry of the emitting species, which provides detailed information on the crystal field splitting and the molecular structure.^{26–28} This also allows for $Eu(III)$ to be used as a structure probe for similar lanthanide complexes.

For $Tb(III)$, the most optically studied $Ln(III)$ after $Eu(III)$, the ground state (7F_6) and main emissive (5D_4) levels consist of 13 and 9 electronic states respectively. The difference in electronic structure of $Tb(III)$ and $Eu(III)$ is illustrated in Fig. 1.

This convolutes the $Tb(III)$ luminescence spectra making deconvoluting the emission bands hard, and as the individual electronic states cannot be resolved, the electronic structure is not readily resolved. Without this information, the optical spectra cannot be correlated to a specific molecular structure.

Over the last decade, we have used molecular photophysics to revisit the electronic structure of several lanthanide ions.^{23,29–40} Due to the reasons laid out above, the focus has been on $Eu(III)$ in particular, where the correlation between molecular structure and photophysics has been investigated in detail for both sensitized europium luminescence,^{31,41,42} and direct excitation.^{29,36,37} While others have aimed to optimize

Department of Chemistry & Nano-Science Center, University of Copenhagen,
Universitetsparken 5, 2100 København Ø, Denmark.

E-mail: nicolaj.kofod@chem.ku.dk, tjs@chem.ku.dk

† Electronic supplementary information (ESI) available: All steady state emission, excitation, time-resolved emission spectra and fitting parameters are given in the ESI. See DOI: <https://doi.org/10.1039/d3dt03657j>

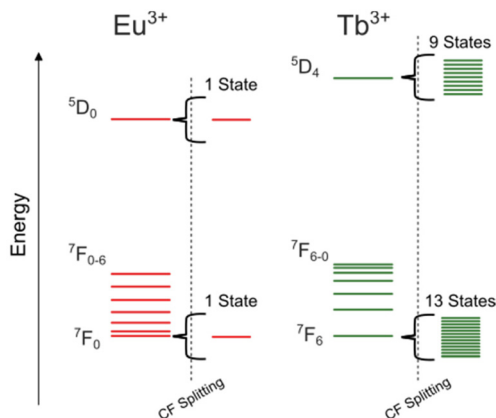


Fig. 1 Illustration showing the number of electronic states within the ground 7F_J and main emissive 5D_J electronic energy levels of Eu(III) and Tb(III) ions (CF = crystal field).

e.g. luminescence sensing,^{43–46} our goal was to establish the molecular structure in solution,^{30,32,33,36,47} in order to determine the photophysical properties of Eu(III) ions in different crystal fields.^{29,36,37} Benchmarking on Eu(III) ³⁴ has allowed us to develop methodologies for analysing optical spectra that can be transferred to other lanthanides.^{23,33,35–37,39} We have revisited complexes of Eu(III) with dipicolinate.^{36,40,48} We have determined quantum yields of luminescence and the radiative rate constants.^{23,29,37} We have investigated the relationship between electronic structure and molecular structure of Dy(III) , Sm(III) , Yb(III) , and Nd(III) ,^{33,35,37,39} and now we turn to Tb(III) .

Despite the apparent complexity of the optical spectra of Tb(III) , we have the methodologies^{33,35,39} to resolve parts of the electronic structure. Tb(III) emission occurs from the 5D_4 emitting level into the seven ${}^7F_{6-0}$ levels. Each level contains $2J + 1$ individual electronic states, split by the crystal field. Depending on the thermal energy and the size of the crystal field splitting, only a certain number of states within the emitting 5D_4 multiplet will be populated.^{33,35} The same is true for the ground state 7F_6 level in absorption. Electronic transitions in both absorption and emission spectroscopy only occur from the populated states within a multiplet. In Tb(III) spectra each observed spectral band is a convolution of the splitting of the final levels and the thermally accessible states of the initial level. In contrast to most of the other lanthanide ions, most Tb(III) transitions involve a number of states that is so high that deconvolution of the spectral bands is difficult if not impossible. For example, the emission around 488 nm from the 5D_4 level into the 7F_6 level contains up to 117 (9·13) individual electronic transitions in a spectral band that often appears with limited fine structure. However, the low energy emission band around 680 nm ($\sim 14\,700\text{ cm}^{-1}$) from ${}^5D_4 \rightarrow {}^7F_0$ transitions is less complicated. The 7F_0 level consists of a single electronic state. This means that the shape of the spectral band is dictated only by the splitting of the emitting 5D_4 level, and that the band contains up to 9 (9·1) individual electronic transitions. That is, the 680 nm band shows the crystal

field splitting of the thermally populated electronic states in the emitting 5D_4 level. In this work, we use this knowledge in combination with high resolution optical spectroscopy to map the electronic structure of the emitting 5D_4 level of four Tb(III) complexes: $[\text{Tb}(\text{H}_2\text{O})_9]^{3+}$, $[\text{Tb}(\text{EDTA})(\text{H}_2\text{O})_3]^-$, $[\text{Tb}(\text{DTPA})(\text{H}_2\text{O})]^{2-}$ and $[\text{Tb}(\text{DOTA})]^-$.

Results and discussion

The structure of the lanthanide(III) aqua ions in solution has been debated in the literature at length.^{49–53} Recently, there has been evidence pointing to the 9-coordinated tricapped trigonal prismatic (TTP) structure being the dominant structure in solution for the Tb(III) aqua ion.^{23,50} The TTP structure has nine oxygen donors in a D_{3h} point group symmetry, see Fig. 2. For the Eu^{3+} analogue this results in a highly symmetric species.^{26,28,37,47}

The $[\text{Ln}(\text{DOTA})(\text{H}_2\text{O})]^-$ complexes has been studied in detail in literature.^{54–64} The molecular structure of $[\text{Ln}(\text{DOTA})(\text{H}_2\text{O})]^-$ complexes can be generalised as a capped square antiprismatic (cSAP) structure with one H_2O acting as a capping ligand with a 4N-4O-1O* donor set, see Fig. 2, where O* denotes oxygen donors from the solvent. This notation is used for all following complexes. Looking closer, the complex exists in an equilibrium between several forms: two nine-coordinated isomers differing in the twist angle between the two 4 atom donor-planes with a capped SAP structure with a twist angle $\sim 39^\circ$ and a twisted capped SAP structure (cTSAP) with a twist angle of $\sim 22^\circ$.^{49,58,62} Traces of the two eight-coordinated, uncapped isomers will also be present, but can often be ignored. For $[\text{Tb}(\text{DOTA})(\text{H}_2\text{O})]^-$ the distribution between the major isomer couple is approx. 9 : 1 cSAP : cTSAP.^{10,39} Note that the C_4 axis of the complex is retained in solution, and that compared to the

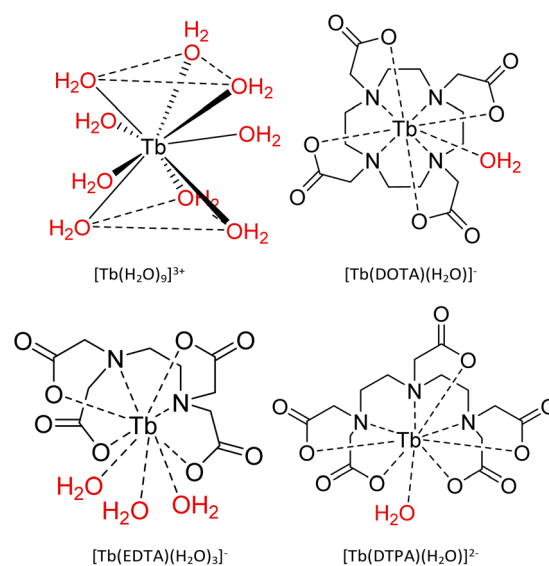


Fig. 2 Complexes used in this study. Inner-sphere water are highlighted in red.

millisecond time-scale of Tb(III) luminescence, these isomers are in fast exchange. Thus, the average luminescence spectrum from the two species will be observed in solution.⁶⁴

The [Tb(EDTA)(H₂O)₃]⁻ complex has a 2N-4O-3O* donor set with three H₂O molecules completing the coordination sphere, see Fig. 3.⁶⁵ The structure is often described as a distorted TTP, but closer inspection reveals that it is neither TTP nor cSAP.⁶⁶ In competitive media, the [Ln(EDTA)(H₂O)₃]⁻ complexes dissociate.^{65,67,68}

[Tb(DTPA)(H₂O)]²⁻ has a 3N-5O-1O* donor set, with a single H₂O molecule completing the coordination sphere, see Fig. 3.⁶⁵ The [Gd(DTPA)(H₂O)]²⁻ was used as a MRI contrast agent, but was banned in 2017 in the EU due to concerns over metal dissociation.^{68,69} As for the EDTA complex, the structure of the DTPA complex lies somewhere between a cSAP and a TTP form.⁶⁵

We recorded the luminescence spectra and time-resolved emission decay profiles for the four Tb³⁺ species, [Tb(H₂O)₉]³⁺, [Tb(EDTA)(H₂O)₃]⁻, [Tb(DTPA)(H₂O)]²⁻ and [Tb(DOTA)(H₂O)]⁻ in H₂O and D₂O. In D₂O, we further recorded the same sample at room temperature (RT) and flash frozen in liquid nitrogen (77 K). Note that all spectra have been normalised as the non-

transparency of the frozen samples does not allow for accurate absolute intensities to be obtained. This data is shown in Fig. 3. Due to the inherently low molar absorption coefficient of Tb(III), absorption spectra were omitted. The excited state lifetimes are compiled in Table 1. All lifetimes show a mono-exponential decay, indicating that all complexations have reached thermodynamic equilibrium and that only one species is present in solution, see Fig. S4, S9, S15 and S21.^{†70} Where the luminescence lifetimes of [Tb(EDTA)(H₂O)₃]⁻ in H₂O and D₂O, and [Tb(DTPA)(H₂O)]²⁻ in H₂O match those found in literature,²⁴ the luminescence lifetimes of [Tb(DTPA)(H₂O)]²⁻ in

Table 1 Excited state lifetimes and number of inner-sphere solvent molecules (*q*) of the four Tb³⁺ complexes in this study

	$\tau_{\text{H}_2\text{O}}$ (ms)	$\tau_{\text{D}_2\text{O}}$ (ms)	<i>q</i>	<i>q</i> lit
[Tb(H ₂ O) ₉] ³⁺	0.425	4.033	10.2	10.1 ^a
[Tb(EDTA)(H ₂ O) ₃] ⁻	1.079	3.547	2.9	2.9 ^b
[Tb(DTPA)(H ₂ O)] ²⁻	1.590	3.153	1.3	1.1 ^b
[Tb(DOTA)(H ₂ O)] ⁻	2.035	3.418	0.7	1.1 ^b

^a Ref. 23. ^b Ref. 24.

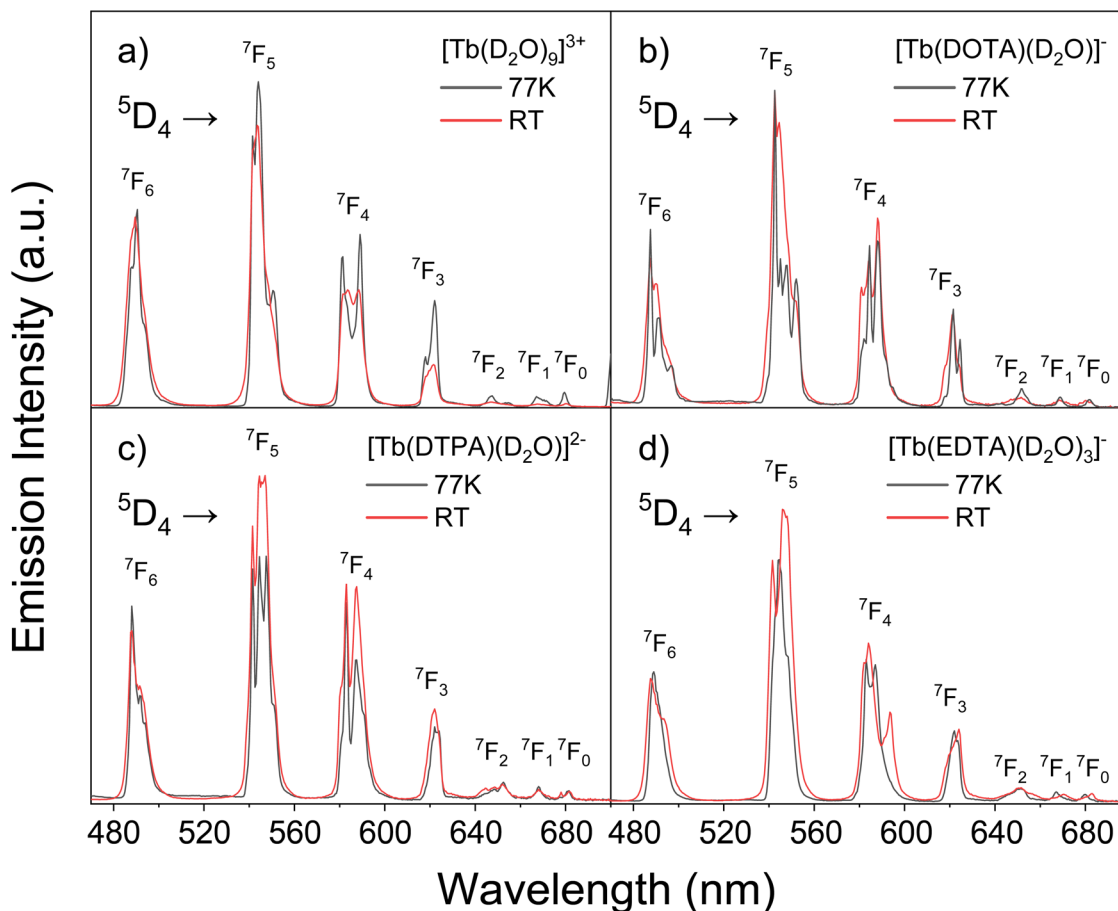


Fig. 3 Emission spectra of 0.1 M [Tb(D₂O)₉]³⁺ (a), 0.05 M [Tb(DOTA)(D₂O)]⁻ (b), 0.05 M [Tb(DTPA)(D₂O)]²⁻ (c) and 0.05 M [Tb(EDTA)(D₂O)₃]⁻ (d) measured in D₂O at 77 K (black) and RT (red). Excitation was done at 372 nm. Excitation slits were kept at 5 nm for all samples. Emission slits were kept at 1 nm for [Tb(D₂O)₉]³⁺, [Tb(DOTA)(D₂O)]⁻, [Tb(DTPA)(D₂O)]²⁻ and 2 nm for [Tb(EDTA)(D₂O)₃]⁻.

D₂O and [Tb(DOTA)(H₂O)]⁻ in H₂O and D₂O are significantly shorter than literature values.²⁴ This could be due differences in pH or differences in proton content of the deuterated solvent. The number of inner-sphere solvent molecules found using the modified Horrocks method match literature values, see Table 1.²⁴

The [Tb(H₂O)₉]³⁺ complex has a *q* value of 10.2 (Table 1), which is above the expected 9 inner-sphere solvent molecules.²³ This discrepancy has been observed before and using an *A* value for the Horrocks equation more suited for non-macrocyclic complexes yields a *q* value of 9.1.²³

We note that the normalized emission spectra of all four complexes in H₂O and D₂O are identical proving that no structural changes happen upon deuterating the solvent, see Fig. S1, S6, S12 and S18.†^{23,37}

Fig. 4 shows the luminescence excitation spectra of the ⁷F₆ → ⁵D₄ transition in the region around 488 nm of the four complexes at RT and 77 K. Closer inspection of these reveals that all four complexes has a blue shift occurs in the ⁷F₆ → ⁵D₄ transition when temperature is decreased. This is because fewer of the 13 ⁷F₆ states are thermally populated at 77 K (Fig. 2).^{33–35,71} The 117 (9·13) individual electronic transitions in ⁷F₆ → ⁵D₄ makes any efforts to elucidate the electronic structure of either level very difficult. Closer investigation of the electronic structure of the emitting ⁵D₄ level requires a more detailed investigation of the emission spectrum.

The Tb(III) luminescence emission spectra consists of seven bands arising from transitions from the ⁵D₄ multiplet into the seven ⁷F₆₋₀ levels, see Fig. 3. The emission spectra is dominated by the first four transitions, ⁵D₄ → ⁷F₆₋₃, with more than 95% of the emission intensity recovered from these bands. Around 680 nm the ⁵D₄ → ⁷F₀ transition can be observed. This

transition is unique in the Tb(III) emission spectra as the ⁷F₀ consists of only a single electronic state. Thus, assuming that the experimental resolution is high enough, the width of the band will be defined by the intrinsic width of the electronic transition and the crystal field splitting of the ⁵D₄ multiplet.^{23,34} Fitting of ⁵D₄ → ⁷F₀ band in the [Tb(H₂O)₉]³⁺, [Tb(EDTA)(H₂O)₃]⁻ and [Tb(DOTA)(H₂O)]⁻ spectra shows that it can be accurately described with a single Lorentzian peak, see Fig. S5, S10 and S22.† The fit parameters are compiled in Table 2. Since the width of the band arises from the splitting of the emitting ⁵D₄ level it follows that the next band, the ⁵D₄ → ⁷F₁ transition, consists of 1–3 peaks with the same width. Fitting the ⁵D₄ → ⁷F₀ and ⁵D₄ → ⁷F₁ bands with Lorentzian peaks results in a good fit for all three complexes. This illustrates that the shape of the emitting ⁵D₄ level is present throughout all Tb(III) emission bands.

It is surprising that the width of the peaks is less than 100 cm⁻¹ in all fits. Either, the emission originates from a single state (or a few close lying states), where the higher-lying states remain beyond thermal population. Or, all the states within the ⁵D₄ level are very close in energy. The first case would give rise to significant hot bands—bands arising from higher lying, thermally populated states—at RT.^{19,72} This is not observed in the emission spectra, where only temperature broadening is observed on the blue side of the bands, when the RT spectra are compared to 77 K spectra. Hot band should be pronounced shoulders on the blue side of each band.³⁴ Therefore, a cluster of nine close lying states within the ⁵D₄

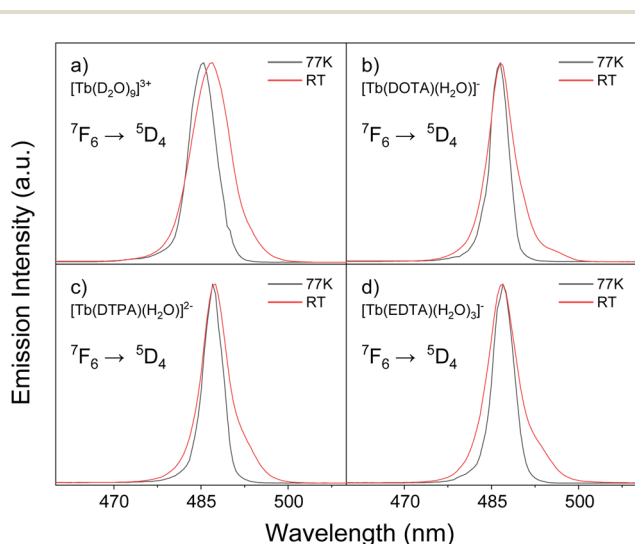


Fig. 4 Normalised excitation spectra of the ⁷F₆ → ⁵D₄ transition of 0.1 M [Tb(D₂O)₉]³⁺ (a), 0.05 M [Tb(DOTA)(H₂O)]⁻ (b), 0.05 M [Tb(DTPA)(H₂O)]²⁻ (c) and 0.05 M [Tb(EDTA)(H₂O)₃]⁻ (d) measured in H₂O or D₂O at 77 K (black) and RT (red). Emission was measured at 545 nm. Emission and excitation slits were kept at 3 nm.

Table 2 Fit parameters of fitted peaks in the ⁵D₄ → ⁷F₀, ⁷F₁ bands of emission

[Tb(H ₂ O) ₉] ³⁺			
Peak #	Peak center (cm ⁻¹)	Peak width ^a (cm ⁻¹)	Peak area
Peak 1	14 717 ± 0.5	59.2 ± 1.2	88.5 ± 1.4
Peak 2	14 990 ± 1.5	59.2 ± 1.2	47.7 ± 2.3
Peak 3	14 943 ± 2.6	59.2 ± 1.2	33.9 ± 2.3
Peak 4	14 890 ± 1.9	59.2 ± 1.2	33.0 ± 1.9
[Tb(EDTA)(H ₂ O) ₃] ⁻			
Peak #	Peak center (cm ⁻¹)	Peak width ^a (cm ⁻¹)	Peak area × 10 ⁵
Peak 1	14 713 ± 0.6	75.2 ± 1.2	43.6 ± 0.56
Peak 2	14 990 ± 0.8	75.2 ± 1.2	40.1 ± 0.76
Peak 3	14 915 ± 2.6	75.2 ± 1.2	11.8 ± 0.68
[Tb(DOTA)(H ₂ O)] ⁻			
Peak #	Peak center (cm ⁻¹)	Peak width ^a (cm ⁻¹)	Peak area × 10 ⁵
Peak 1	14 670 ± 0.9	62.8 ± 1.6	9.68 ± 0.23
Peak 2	14 953 ± 0.8	62.8 ± 1.6	12.0 ± 0.25
[Tb(DTPA)(H ₂ O)] ²⁻			
Peak #	Peak center (cm ⁻¹)	Peak width ^a (cm ⁻¹)	Peak area × 10 ⁵
Peak 1	14 688 ± 1.1	59.1 ± 3.3	19.4 ± 0.86
Peak 2	14 763 ± 6.0	59.1 ± 3.3	3.75 ± 0.60
Peak # (RT)			
Peak #	Peak center (cm ⁻¹)	Peak width ^a (cm ⁻¹)	Peak area × 10 ⁵
Peak 1	14 676 ± 1.0	59.8 ± 2.2	16.1 ± 0.46
Peak 2	14 754 ± 1.3	59.8 ± 2.2	12.2 ± 0.41

^a Shared parameter.

multiplet appears to be the most likely explanation. A total crystal field splitting of less than 100 cm^{-1} is small, even for a lanthanide.^{33,72} For the ground state multiplet, 7F_6 , crystal field splitting on the order of several hundred cm^{-1} are known, and there are several examples of crystal field splitting exceeding 1000 cm^{-1} .⁷³

Detailed crystal field studies of lanthanide complexes are usually performed with single-molecule magnets in mind, a field where the ground state level is of primary interest. Studies with the crystal field splitting of the high lying emissive levels as a focus are rare, except for a few studies focusing on Yb^{3+} .^{33,71,74–78} Comparisons of crystal field splitting in higher lying levels are therefore limited. However, ‘hot’ emission lines, which arise from higher lying states within the emitting level, have been observed around 100 cm^{-1} above the main emission line.^{19,72} Thus, we can conclude that the band shape of the ${}^5D_4 \rightarrow {}^7F_0$ can be used to map the emitting level of Tb(III) . And we note that the nine states of the 5D_4 level in $[\text{Tb}(\text{H}_2\text{O})_9]^{3+}$, $[\text{Tb}(\text{EDTA})(\text{H}_2\text{O})_3]^-$ and $[\text{Tb}(\text{DOTA})(\text{H}_2\text{O})]^-$ must be spaced by mere tens of reciprocal centimetres, in an envelope with a width $<100\text{ cm}^{-1}$. Fig. 5 shows the spectral shape and energy levels determined for the $[\text{Tb}(\text{H}_2\text{O})_9]^{3+}$, $[\text{Tb}(\text{EDTA})(\text{H}_2\text{O})_3]^-$ and $[\text{Tb}(\text{DOTA})(\text{H}_2\text{O})]^-$ complexes. It should be noted that the choice of a Lorentzian function for the fit is not trivial. We have previously shown that the peak shape of lanthanide optical transitions can be described by either Lorentzian, Gaussian or a Voigt function depending on the system and conditions.^{23,30,34,35} Based on these studies this case should ideally be described by a Voigt function, but we find this overfits the data. A Gaussian function fits the ${}^5D_4 \rightarrow {}^7F_1$ slightly better and reduces the number of peaks in the $[\text{Tb}(\text{H}_2\text{O})_9]^{3+} {}^5D_4 \rightarrow {}^7F_1$ band to two peaks. However, since the quality of fit of the ${}^5D_4 \rightarrow {}^7F_0$ band is significantly reduced for all four complexes, we chose to proceed with the Lorentzian fit.

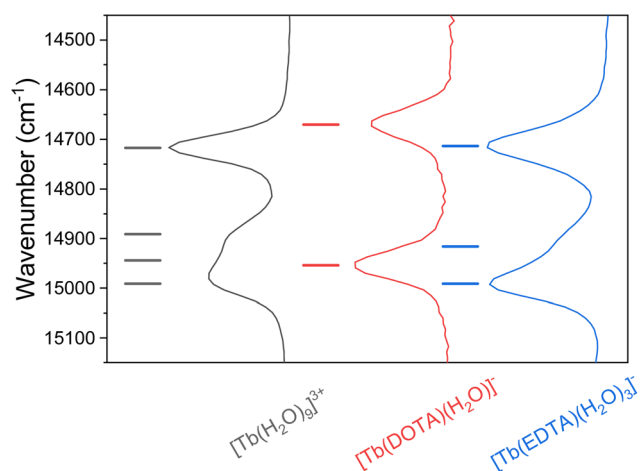


Fig. 5 Emission spectra of the ${}^5D_4 \rightarrow {}^7F_0$, 7F_1 bands of $[\text{Tb}(\text{H}_2\text{O})_9]^{3+}$ (black), $[\text{Tb}(\text{DOTA})(\text{H}_2\text{O})]^-$ (red) and $[\text{Tb}(\text{EDTA})(\text{H}_2\text{O})_3]^-$ (red). The lines indicate the energy of the individual electronic states determined by fitting the data to Lorentzian functions (see main text).

The $[\text{Tb}(\text{DTPA})(\text{H}_2\text{O})]^{2-}$ complex is different. Here, the ${}^5D_4 \rightarrow {}^7F_0$ transition has two bands separated by $\sim 75\text{ cm}^{-1}$, see Fig. 6. The two bands are present in both the RT and 77 K data, but varying in relative intensities as a function of temperature. In both RT and 77 K spectra, the bands are accurately fitted by two Lorentzian functions with a shared width. The fit parameters are compiled in Table S3.† We note that the relative area of the bands at 77 K and at RT closely match the expected Boltzmann distribution between two energy levels split by the difference between the two band center energies. This indicates that the emitting 5D_4 level must consist of two groups of states separated by $\sim 75\text{ cm}^{-1}$. It should be noted that the Boltzmann treatment is done considering only two states. The 5D_4 multiplet contains nine individual states, and assuming that no high-lying states exist (see above), the more likely explanation is that the groups of states contain 5 and 4 states each. There is no way to determine, which group has 4 states and which has 5 states from the experimental results. As changing the number of states in the Boltzmann analysis gives only slight changes in the determined populations, any further assignment would be purely speculative. The standard deviation between the 2 state model and one with 9 states in either a 4/5 or 5/4 arrangement is 2.9% and 4.4% for the 77 K and RT data respectively. This deviation is well within the experimental uncertainty. Note that models with other arrangements of states, e.g. 1/8, 2/7 etc. are not consistent with the experimental results and can therefore be excluded. The spectral resolution does not allow for the two sets of transitions to be observed in the ${}^5D_4 \rightarrow {}^7F_1$ band, see Fig. S17.†

An alternative explanation would be that the $[\text{Tb}(\text{DTPA})(\text{H}_2\text{O})]^{2-}$ complex exists as two different isomers in solution, that is two molecular structures in slow exchange. This is usually the first conclusion drawn from multiple lines in the ${}^5D_0 \rightarrow {}^7F_0$ transition in Eu(III) where the emitting level

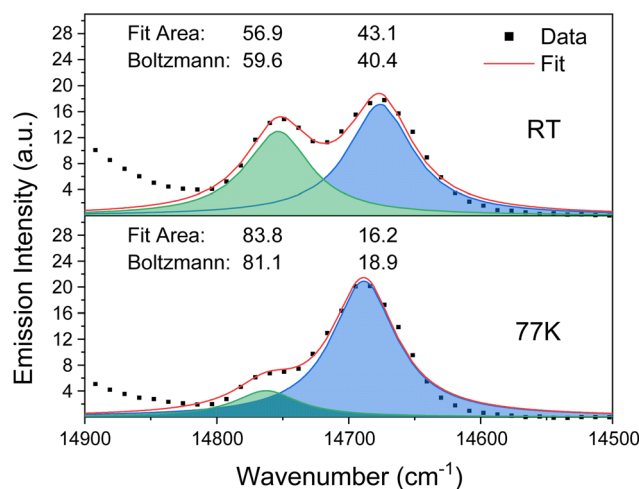


Fig. 6 Emission spectra of the ${}^5D_4 \rightarrow {}^7F_0$ transition of $[\text{Tb}(\text{DTPA})(\text{D}_2\text{O})]^-$ in D_2O at RT (top) and 77 K (bottom). The area of the fitted peak as well as the calculated Boltzmann distribution for a two state system (see main text for details) is given in the figure.

has only one state and any explanation invoking split states are invalid.^{26,36} However, there are two arguments against this explanation. First, it is unlikely that the two structures would have an energy difference that (i) closely matching the spectral energy difference of the bands and (ii) that is so small. Second, it seems unreasonable that the two isomers with an energy difference of 75 cm⁻¹ would have an exchange slower than the millisecond timescale of the excited state lifetime.

Thus, we can conclude that the emitting ⁵D₄ level of the [Tb(DTPA)(H₂O)]²⁻ complex consists of two groups of states separated by ~75 cm⁻¹, each group giving rise to a separate emission band in the ⁵D₄ → ⁷F₀ transition. It is noteworthy that of the four complexes studied, this behaviour is only observed for the [Tb(DTPA)(H₂O)]²⁻ complex here. As both the [Tb(DTPA)(H₂O)]²⁻ and [Tb(EDTA)(H₂O)₃]⁻ complexes have low symmetry, it would be expected that the [Tb(EDTA)(H₂O)₃]⁻ would have similar properties. Clearly, this is not the case.

Conclusions

The spectroscopic characterization of the [Tb(H₂O)₉]³⁺, [Tb(EDTA)(H₂O)₃]⁻, [Tb(DTPA)(H₂O)]²⁻ and [Tb(DOTA)(H₂O)]⁻ complexes was performed in H₂O and D₂O. The four complexes show significant changes in the band shape when cooled from room temperature to 77 K. This was assigned to a change in the thermally populated states within the absorbing and/or main emissive energy levels. High-resolution emission spectra of the ⁵D₄ → ⁷F₀ transition revealed the distribution of states within the ⁵D₄ level. For the [Tb(H₂O)₉]³⁺, [Tb(EDTA)(H₂O)₃]⁻, and [Tb(DOTA)(H₂O)]⁻ complexes we found that the individual states within the ⁵D₄ level lies as a single group of nine states with a total crystal field splitting significantly less than 100 cm⁻¹. For the [Tb(DTPA)(H₂O)]²⁻ complex we found that the nine states of the ⁵D₄ state were separated into two groups separated by ~75 cm⁻¹. Additionally we found that knowing the distribution of electronic states in the ⁵D₄ level can be used to determine if the fine structure of the bands in the full emission spectra of Tb(III) complexes arises in the ⁷F₇ state or is due to crystal field splitting in ⁵D₄.

Experimental section

All materials were used as received: Tb(CF₃SO₃)₃ (98%, Strem Chemicals), H₄EDTA (own supply, ¹H-NMR in Fig. S11†), H₄DOTA (Sigma Aldrich), H₅DTPA (CheMatec). D₂O (99.90% D, Eurisotop), and H₂O (from a Milli-Q purification system at 18.2 Ω) were used as solvents. pH/pD was adjusted using NaOH from common vendors or NaOD from Eurisotop. All solutions were made without buffers.

[Tb(H₂O)₉]³⁺/[Tb(D₂O)₉]³⁺

A 0.1 M solution of [Tb(H₂O)₉]³⁺ was prepared by dissolving 303.4 ± 0.2 mg of Tb(CF₃SO₃)₃ in 5 mL solvent.

[Tb(EDTA)(H₂O)₃]⁻

A 0.05 M solution of [Tb(EDTA)(H₂O)₃]⁻ was prepared by adding 91.95/92.8 mg of TbCl₃ and 73.24/74.74 mg of H₄EDTA to 5 mL of solvent for the H₂O and D₂O samples respectively. The samples were sealed and stirred for 2 days at 60 °C before measuring.

[Tb(DTPA)(H₂O)]²⁻

A 0.05 M solution of [Tb(DTPA)(H₂O)]²⁻ was prepared by adding 94.30/92.23 mg of TbCl₃ and 98.60/98.07 mg of H₅DTPA to 5 mL solvent for the H₂O and D₂O samples respectively with pH/pD adjusted to ~5 using NaOH/NaOD. The samples were sealed and stirred for 4 days at 60 °C before measuring.

[Tb(DOTA)(H₂O)]⁻

A 0.05 M solution of [Tb(DOTA)(H₂O)]⁻ was prepared by dissolving 302.11/301.70 mg of Tb(CF₃SO₃)₃ and 201.05/203.85 mg of H₄DOTA in 10 mL of solvent for the H₂O and D₂O samples respectively with pH/pD adjusted to ~5 using NaOH/NaOD. The samples were sealed and stirred for 4 days at 60 °C for 4 days before measuring.

Spectroscopy

All steady-state and time-resolved emission and excitation spectra were recorded on a PTI QuantaMaster8075 from Horiba Scientific using the built-in xenon arc lamps for excitation. All room-temperature samples were measured in 10 mm quartz cuvettes from Starna Scientific. Cooled samples were measured in standard NMR tubes placed in a quartz Dewar from Horiba Scientific filled with liquid nitrogen. The excitation and emission slits varied for the different measurements. The specific width is noted in the caption of each spectrum. Corrections for lamp fluctuations and wavelength-dependent detector sensibility were done by using the factory provided correction files. A constant flow of nitrogen was sent through the sample chamber to avoid condensation.

Conflicts of interest

There are no conflicts to declare.

Acknowledgements

The authors thank the Novo Nordisk Foundation, The Villum Foundation (Grant No. 14922), The Carlsberg Foundation (CF23-0104, CF15-0171 & CF20-0089), The University of Copenhagen and Fulbright Denmark for support. The authors also thank Dr Lea Gundorff Nielsen for her help in preparing this manuscript.

References

- 1 R. Arppe and T. J. Sørensen, Physical unclonable functions generated through chemical methods for anti-counterfeiting, *Nat. Rev. Chem.*, 2017, **1**(4), 0031, DOI: [10.1038/s41570-017-0031](https://doi.org/10.1038/s41570-017-0031).
- 2 E. Pershagen and K. E. Borbas, Designing reactivity-based responsive lanthanide probes for multicolor detection in biological systems, *Coord. Chem. Rev.*, 2014, **273**, 30–46.
- 3 C. P. Montgomery, B. S. Murray, E. J. New, R. Pal and D. Parker, Cell-Penetrating Metal Complex Optical Probes: Targeted and Responsive Systems Based on Lanthanide Luminescence, *Acc. Chem. Res.*, 2009, **42**(7), 925–937, DOI: [10.1021/ar800174z](https://doi.org/10.1021/ar800174z).
- 4 R. Arppe-Tabbara, M. Tabbara and T. J. Sørensen, Versatile and Validated Optical Authentication System Based on Physical Unclonable Functions, *ACS Appl. Mater. Interfaces*, 2019, **11**(6), 6475–6482, DOI: [10.1021/acsami.8b17403](https://doi.org/10.1021/acsami.8b17403).
- 5 S. V. Eliseeva and J.-C. G. Bünzli, Lanthanide luminescence for functional materials and bio-sciences, *Chem. Soc. Rev.*, 2010, **39**(1), 189–227, DOI: [10.1039/B905604C](https://doi.org/10.1039/B905604C).
- 6 M. C. Heffern, L. M. Matosziuk and T. J. Meade, Lanthanide Probes for Bioresponsive Imaging, *Chem. Rev.*, 2014, **114**(8), 4496–4539, DOI: [10.1021/cr400477t](https://doi.org/10.1021/cr400477t).
- 7 I. Hemmilä, S. Dakubu, V.-M. Mikkala, H. Siitari and T. Lövgren, Europium as a label in time-resolved immunofluorometric assays, *Anal. Biochem.*, 1984, **137**(2), 335–343, DOI: [10.1016/0003-2697\(84\)90095-2](https://doi.org/10.1016/0003-2697(84)90095-2).
- 8 A. de Bettencourt-Dias, Lanthanide-based emitting materials in light-emitting diodes, *Dalton Trans.*, 2007, (22), 2229–2241, DOI: [10.1039/B702341C](https://doi.org/10.1039/B702341C).
- 9 W. R. Algar, D. Wegner, A. L. Huston, J. B. Blanco-Canosa, M. H. Stewart, A. Armstrong, P. E. Dawson, N. Hildebrandt and I. L. Medintz, Quantum dots as simultaneous acceptors and donors in time-gated forster resonance energy transfer relays: characterization and biosensing, *J. Am. Chem. Soc.*, 2012, **134**(3), 1876–1891.
- 10 C. Chen, B. Corry, L. Huang and N. Hildebrandt, FRET-modulated multihybrid nanoparticles for brightness-equalized single-wavelength barcoding, *J. Am. Chem. Soc.*, 2019, **141**(28), 11123–11141.
- 11 S. A. Díaz, G. Lasarte Aragonés, S. Buckhout-White, X. Qiu, E. Oh, K. Susumu, J. S. Melinger, A. L. Huston, N. Hildebrandt and I. L. Medintz, Bridging Lanthanide to Quantum Dot Energy Transfer with a Short-Lifetime Organic Dye, *J. Phys. Chem. Lett.*, 2017, **8**(10), 2182–2188, DOI: [10.1021/acs.jpcclett.7b00584](https://doi.org/10.1021/acs.jpcclett.7b00584).
- 12 N. Hildebrandt, K. D. Wegner and W. R. Algar, Luminescent terbium complexes: Superior Förster resonance energy transfer donors for flexible and sensitive multiplexed biosensing, *Coord. Chem. Rev.*, 2014, **273**, 125–138.
- 13 X. Qiu, J. Xu, M. Cardoso Dos Santos and N. Hildebrandt, Multiplexed Biosensing and Bioimaging Using Lanthanide-Based Time-Gated Förster Resonance Energy Transfer, *Acc. Chem. Res.*, 2022, **55**(4), 551–564, DOI: [10.1021/acs.accounts.1c00691](https://doi.org/10.1021/acs.accounts.1c00691).
- 14 M. Sy, A. Nonat, N. Hildebrandt and L. J. Charbonnière, Lanthanide-based luminescence biolabelling, *Chem. Commun.*, 2016, **52**(29), 5080–5095.
- 15 J. M. Zwier and N. Hildebrandt, Time-gated FRET detection for multiplexed biosensing, in *Reviews in fluorescence 2016*, Springer, 2017, pp. 17–43.
- 16 M. Dekaliuk and N. Hildebrandt, Lanthanide-FRET molecular beacons for microRNA biosensing, logic operations, and physical unclonable functions, *Eur. J. Inorg. Chem.*, 2017, e202300288, DOI: [10.1002/ejic.202300288](https://doi.org/10.1002/ejic.202300288).
- 17 A. D'Aléo, G. Pompidor, B. Elena, J. Vicat, P. L. Baldeck, L. Toupet, R. Kahn, C. Andraud and O. Maury, Two-Photon Microscopy and Spectroscopy of Lanthanide Bioprobes, *ChemPhysChem*, 2007, **8**(14), 2125–2132, DOI: [10.1002/cphc.200700375](https://doi.org/10.1002/cphc.200700375).
- 18 A. T. Bui, A. Roux, A. Grichine, A. Duperray, C. Andraud and O. Maury, Twisted Charge-Transfer Antennae for Ultra-Bright Terbium(III) and Dysprosium(III) Bioprobes, *Chem. – Eur. J.*, 2018, **24**(14), 3408–3412, DOI: [10.1002/chem.201705933](https://doi.org/10.1002/chem.201705933).
- 19 J. Wang, J. J. Zakrzewski, M. Zychowicz, Y. Xin, H. Tokoro, S. Chorazy and S.-I. Ohkoshi, Desolvation-Induced Highly Symmetrical Terbium(III) Single-Molecule Magnet Exhibiting Luminescent Self-Monitoring of Temperature, *Angew. Chem., Int. Ed.*, 2023, e202306372.
- 20 S. Demir, M. I. Gonzalez, L. E. Darago, W. J. Evans and J. R. Long, Giant coercivity and high magnetic blocking temperatures for N23– radical-bridged dilanthanide complexes upon ligand dissociation, *Nat. Commun.*, 2017, **8**(1), 2144, DOI: [10.1038/s41467-017-01553-w](https://doi.org/10.1038/s41467-017-01553-w).
- 21 M. Gonidec, R. Biagi, V. Corradini, F. Moro, V. De Renzi, U. del Pennino, D. Summa, L. Muccioli, C. Zannoni, D. B. Amabilino and J. Veciana, Surface Supramolecular Organization of a Terbium(III) Double-Decker Complex on Graphite and its Single Molecule Magnet Behavior, *J. Am. Chem. Soc.*, 2011, **133**(17), 6603–6612, DOI: [10.1021/ja109296c](https://doi.org/10.1021/ja109296c).
- 22 J. D. Rinehart, M. Fang, W. J. Evans and J. R. Long, A N23– Radical-Bridged Terbium Complex Exhibiting Magnetic Hysteresis at 14 K, *J. Am. Chem. Soc.*, 2011, **133**(36), 14236–14239, DOI: [10.1021/ja206286h](https://doi.org/10.1021/ja206286h).
- 23 N. Kofod and T. J. Sørensen, Tb3+ Photophysics: Mapping Excited State Dynamics of [Tb(H2O)9]3+ Using Molecular Photophysics, *J. Phys. Chem. Lett.*, 2022, **13**(51), 11968–11973, DOI: [10.1021/acs.jpcclett.2c03506](https://doi.org/10.1021/acs.jpcclett.2c03506).
- 24 A. Beeby, M. Clarkson, I. S. R. Dickins, S. Faulkner, D. Parker, L. S. Royle, A. A. de Sousa, J. Gareth Williams and M. Woods, Non-radiative deactivation of the excited states of europium, terbium and ytterbium complexes by proximate energy-matched OH, NH and CH oscillators: an improved luminescence method for establishing solution hydration states, *J. Chem. Soc., Perkin Trans. 2*, 1999, (3), 493–504, DOI: [10.1039/A808692C](https://doi.org/10.1039/A808692C).
- 25 W. D. Horrocks Jr. and D. R. Sudnick, Lanthanide ion probes of structure in biology. Laser-induced luminescence decay constants provide a direct measure of the number of

- metal-coordinated water molecules, *J. Am. Chem. Soc.*, 1979, **101**(2), 334–340.
- 26 K. Binnemans, Interpretation of europium(III) spectra, *Coord. Chem. Rev.*, 2015, **295**, 1–45, DOI: [10.1016/j.ccr.2015.02.015](https://doi.org/10.1016/j.ccr.2015.02.015).
- 27 A. de Bettencourt-Dias, *Luminescence of lanthanide ions in coordination compounds and nanomaterials*, John Wiley & Sons, 2014.
- 28 P. A. Tanner, Some misconceptions concerning the electronic spectra of tri-positive europium and cerium, *Chem. Soc. Rev.*, 2013, **42**(12), 5090–5101, DOI: [10.1039/C3CS60033E](https://doi.org/10.1039/C3CS60033E).
- 29 N. Kofod, L. G. Nielsen and T. J. Sørensen, Temperature Dependence of Fundamental Photophysical Properties of $[\text{Eu}(\text{MeOH-d}_4)_9]^{3+}$ Solvates and $[\text{Eu}\cdot\text{DOTA}(\text{MeOH-d}_4)]^-$ Complexes, *J. Phys. Chem. A*, 2021, **125**(38), 8347–8357, DOI: [10.1021/acs.jpca.1c04994](https://doi.org/10.1021/acs.jpca.1c04994).
- 30 N. Kofod, P. Nawrocki, M. Juelsholt, T. L. Christiansen, K. MØ. Jensen and T. J. Sørensen, Solution Structure, Electronic Energy Levels, and Photophysical Properties of $[\text{Eu}(\text{MeOH})_{n-2m}(\text{NO}_3)_m]^{3-m+}$ Complexes, *Inorg. Chem.*, 2020, **59**(15), 10409–10421, DOI: [10.1021/acs.inorgchem.0c00056](https://doi.org/10.1021/acs.inorgchem.0c00056).
- 31 A. K. R. Junker, L. R. Hill, A. L. Thompson, S. Faulkner and T. J. Sørensen, Shining light on the antenna chromophore in lanthanide based dyes, *Dalton Trans.*, 2018, **47**(14), 4794–4803.
- 32 N. Kofod, M. Storm Thomsen, P. Nawrocki and T. J. Sørensen, Revisiting the assignment of innocent and non-innocent counterions in lanthanide(III) solution chemistry, *Dalton Trans.*, 2022, **51**(20), 7936–7949, DOI: [10.1039/D2DT00565D](https://doi.org/10.1039/D2DT00565D).
- 33 N. Kofod, P. Nawrocki, C. Platas-Iglesias and T. J. Sørensen, Electronic Structure of Ytterbium(III) Solvates—a Combined Spectroscopic and Theoretical Study, *Inorg. Chem.*, 2021, **60**(10), 7453–7464, DOI: [10.1021/acs.inorgchem.1c00743](https://doi.org/10.1021/acs.inorgchem.1c00743).
- 34 V. R. M. Nielsen, P. R. Nawrocki and T. J. Sørensen, Electronic Structure of Neodymium(III) and Europium(III) Resolved in Solution Using High-Resolution Optical Spectroscopy and Population Analysis, *J. Phys. Chem. A*, 2023, **127**(16), 3577–3590, DOI: [10.1021/acs.jpca.3c00233](https://doi.org/10.1021/acs.jpca.3c00233).
- 35 N. Kofod, R. Arppe-Tabbara and T. J. Sørensen, Electronic Energy Levels of Dysprosium(III) ions in Solution. Assigning the Emitting State and the Intraconfigurational 4f–4f Transitions in the Vis–NIR Region and Photophysical Characterization of Dy(III) in Water, Methanol, and Dimethyl Sulfoxide, *J. Phys. Chem. A*, 2019, **123**(13), 2734–2744, DOI: [10.1021/acs.jpca.8b12034](https://doi.org/10.1021/acs.jpca.8b12034).
- 36 P. R. Nawrocki, N. Kofod, M. Juelsholt, K. M. Jensen and T. J. Sørensen, The effect of weighted averages when determining the speciation and structure–property relationships of europium(III) dipicolinate complexes, *Phys. Chem. Chem. Phys.*, 2020, **22**(22), 12794–12805, DOI: [10.1039/D0CP00989J](https://doi.org/10.1039/D0CP00989J).
- 37 N. Kofod, P. Nawrocki and T. J. Sørensen, Arel: Investigating $[\text{Eu}(\text{H}_2\text{O})_9]^{3+}$ Photophysics and Creating a Method to Bypass Luminescence Quantum Yield Determinations, *J. Phys. Chem. Lett.*, 2022, **13**(13), 3096–3104, DOI: [10.1021/acs.jpcclett.2c00418](https://doi.org/10.1021/acs.jpcclett.2c00418).
- 38 P. R. Nawrocki and T. J. Sørensen, Optical spectroscopy as a tool for studying the solution chemistry of neodymium(III), *Phys. Chem. Chem. Phys.*, 2023, **25**(29), 19300–19336, DOI: [10.1039/D3CP02033A](https://doi.org/10.1039/D3CP02033A).
- 39 S. S. Mortensen, M. A. Marciniak Nielsen, P. Nawrocki and T. J. Sørensen, Electronic Energy Levels and Optical Transitions in Samarium(III) Solvates, *J. Phys. Chem. A*, 2022, **126**(46), 8596–8605, DOI: [10.1021/acs.jpca.2c04793](https://doi.org/10.1021/acs.jpca.2c04793).
- 40 S. S. Mortensen and T. J. Sørensen, Crystal structures of two SmIII complexes with dipicolinate [DPA]²⁻ ligands: comparison of luminescent properties of products obtained at different pH values, *Acta Crystallogr., Sect. E: Crystallogr. Commun.*, 2023, **79**(7), 619–625, DOI: [10.1107/S2056989023004814](https://doi.org/10.1107/S2056989023004814).
- 41 D. Kovacs and K. E. Borbas, The role of photoinduced electron transfer in the quenching of sensitized Europium emission, *Coord. Chem. Rev.*, 2018, **364**, 1–9, DOI: [10.1016/j.ccr.2018.03.004](https://doi.org/10.1016/j.ccr.2018.03.004).
- 42 A. G. Cosby, J. J. Woods, P. Nawrocki, T. J. Sørensen, J. J. Wilson and E. Boros, Accessing lanthanide-based, in situ illuminated optical turn-on probes by modulation of the antenna triplet state energy, *Chem. Sci.*, 2021, **12**(27), 9442–9451, DOI: [10.1039/D1SC02148F](https://doi.org/10.1039/D1SC02148F).
- 43 D. Kocsi, A. Orthaber and K. E. Borbas, Tuning the photophysical properties of luminescent lanthanide complexes through regioselective antenna fluorination, *Chem. Commun.*, 2022, **58**(48), 6853–6856, DOI: [10.1039/D2CC01229D](https://doi.org/10.1039/D2CC01229D).
- 44 E. Pershagen, J. Nordholm and K. E. Borbas, Luminescent Lanthanide Complexes with Analyte-Triggered Antenna Formation, *J. Am. Chem. Soc.*, 2012, **134**(24), 9832–9835, DOI: [10.1021/ja3004045](https://doi.org/10.1021/ja3004045).
- 45 D. Kovacs, X. Lu, L. S. Meszaros, M. Ott, J. Andres and K. E. Borbas, Photophysics of coumarin and carbostyryl-sensitized luminescent lanthanide complexes: implications for complex design in multiplex detection, *J. Am. Chem. Soc.*, 2017, **139**(16), 5756–5767.
- 46 J. Andres and K. E. Borbas, Expanding the Versatility of Dipicolinate-Based Luminescent Lanthanide Complexes: A Fast Method for Antenna Testing, *Inorg. Chem.*, 2015, **54**(17), 8174–8176, DOI: [10.1021/acs.inorgchem.5b01579](https://doi.org/10.1021/acs.inorgchem.5b01579).
- 47 M. Storm Thomsen, P. R. Nawrocki, N. Kofod and T. J. Sørensen, Seven Europium(III) Complexes in Solution – the Importance of Reporting Data When Investigating Luminescence Spectra and Electronic Structure, *Eur. J. Inorg. Chem.*, 2022, e202200334, DOI: [10.1002/ejic.202200334](https://doi.org/10.1002/ejic.202200334).
- 48 S. S. Mortensen and T. J. Sørensen, Nine-coordinated Eu³⁺ Dipicolinate Compounds: Different Crystal Structures and Luminescence Properties as a Function of pH, *Eur. J. Inorg. Chem.*, 2023, e202300159, DOI: [10.1002/ejic.202300159](https://doi.org/10.1002/ejic.202300159).
- 49 L. Helm and A. E. Merbach, Inorganic and bioinorganic solvent exchange mechanisms, *Chem. Rev.*, 2005, **105**(6), 1923–1959, DOI: [10.1021/cr030726o](https://doi.org/10.1021/cr030726o).

- 50 I. Persson, P. D'Angelo, S. De Panfilis, M. Sandström and L. Eriksson, Hydration of Lanthanoid(III) Ions in Aqueous Solution and Crystalline Hydrates Studied by EXAFS Spectroscopy and Crystallography: The Myth of the "Gadolinium Break", *Chem. – Eur. J.*, 2008, **14**(10), 3056–3066, DOI: [10.1002/chem.200701281](https://doi.org/10.1002/chem.200701281).
- 51 C. Cossy, A. C. Barnes, J. E. Enderby and A. E. Merbach, The hydration of Dy³⁺ and Yb³⁺ in aqueous solution: A neutron scattering first order difference study, *J. Chem. Phys.*, 1989, **90**(6), 3254–3260.
- 52 C. Cossy, L. Helm, D. H. Powell and A. E. Merbach, A change in coordination number from nine to eight along the lanthanide (III) aqua ion series in solution: a neutron diffraction study, *New J. Chem.*, 1995, **19**, 27–35.
- 53 T. Yamaguchi, M. Nomura, H. Wakita and H. Ohtaki, An extended x-ray absorption fine structure study of aqueous rare earth perchlorate solutions in liquid and glassy states, *J. Chem. Phys.*, 1988, **89**(8), 5153–5159.
- 54 J. F. Desreux, Nuclear magnetic resonance spectroscopy of lanthanide complexes with a tetraacetic tetraaza macrocycle. Unusual conformation properties, *Inorg. Chem.*, 1980, **19**(5), 1319–1324.
- 55 S. Aime, M. Botta and G. Ermondi, NMR study of solution structures and dynamics of lanthanide(III) complexes of DOTA, *Inorg. Chem.*, 1992, **31**(21), 4291–4299.
- 56 S. Aime, A. Barge, M. Botta, M. Fasano, J. D. Ayala and G. Bombieri, Crystal structure and solution dynamics of the lutetium(III) chelate of DOTA, *Inorg. Chim. Acta*, 1996, **246**(1–2), 423–429.
- 57 V. Jacques and J. F. Desreux, Quantitative two-dimensional EXSY spectroscopy and dynamic behavior of a paramagnetic lanthanide macrocyclic chelate: YbDOTA (DOTA = 1, 4, 7, 10-tetraazacyclododecane-N, N', N'', N'''-tetraacetic acid), *Inorg. Chem.*, 1994, **33**(18), 4048–4053.
- 58 S. Hoeft and K. Roth, Struktur und Dynamik von Lanthanoid-Tetraazacyclododecantetraacetat-(DOTA-) Komplexen in Lösung, *Chem. Ber.*, 1993, **126**(4), 869–873.
- 59 J. A. Peters, K. Djanashvili, C. F. G. C. Geraldes and C. Platas-iglesias, Structure, Dynamics, and Computational Studies of Lanthanide-Based Contrast Agents, in *The chemistry of contrast agents in medical magnetic resonance imaging*, 2013, pp. 209–276.
- 60 S. Aime, M. Botta, M. Fasano, M. P. M. Marques, C. F. G. C. Geraldes, D. Pubanz and A. E. Merbach, Conformational and coordination equilibria on DOTA complexes of lanthanide metal ions in aqueous solution studied by ¹H-NMR spectroscopy, *Inorg. Chem.*, 1997, **36**(10), 2059–2068.
- 61 M. Storm Thomsen, H. O. B. Andersen and T. J. Sørensen, Long story short: donor set symmetry in [Eu(DOTA)(H₂O)]⁻ crystals determines the electronic structure, *Dalton Trans.*, 2022, **51**, 14118–14124, DOI: [10.1039/D2DT02172B](https://doi.org/10.1039/D2DT02172B).
- 62 M. Storm Thomsen, S. Parsons and T. J. Sørensen, Invisible strings. The first single crystal of the cTSAP form of [Eu(DOTA)(H₂O)]⁻ has an electronic structure similar to one of the reported cSAP forms, *Dalton Trans.*, 2022, **51**(41), 15725–15733, DOI: [10.1039/D2DT02633C](https://doi.org/10.1039/D2DT02633C).
- 63 M. Woods, S. Aime, M. Botta, J. A. K. Howard, J. M. Moloney, M. Navet, D. Parker, M. Port and O. Rousseaux, Correlation of water exchange rate with isomeric composition in diastereoisomeric gadolinium complexes of tetra (carboxyethyl) dota and related macrocyclic ligands, *J. Am. Chem. Soc.*, 2000, **122**(40), 9781–9792.
- 64 L. G. Nielsen and T. J. Sørensen, Including and Declaring Structural Fluctuations in the Study of Lanthanide(III) Coordination Chemistry in Solution, *Inorg. Chem.*, 2019, **59**(1), 94–105, DOI: [10.1021/acs.inorgchem.9b01571](https://doi.org/10.1021/acs.inorgchem.9b01571).
- 65 P. Caravan, J. J. Ellison, T. J. McMurphy and R. B. Lauffer, Gadolinium(III) chelates as MRI contrast agents: Structure, dynamics, and applications, *Chem. Rev.*, 1999, **99**(9), 2293–2352, DOI: [10.1021/Cr980440x](https://doi.org/10.1021/Cr980440x).
- 66 S. Faulkner and O. A. Blackburn, The Chemistry of Lanthanide MRI Contrast Agents, in *The Chemistry of Molecular Imaging*, 2014, pp. 179–197.
- 67 P. Wedeking, K. Kumar and M. F. Tweedle, Dissociation of gadolinium chelates in mice: relationship to chemical characteristics, *Magn. Reson. Imaging*, 1992, **10**(4), 641–648.
- 68 T. J. Sørensen and S. Faulkner, Multimetallic Lanthanide Complexes: Using Kinetic Control To Define Complex Multimetallic Arrays, *Acc. Chem. Res.*, 2018, **51**(10), 2493–2501, DOI: [10.1021/acs.accounts.8b00205](https://doi.org/10.1021/acs.accounts.8b00205).
- 69 M. A. H. P. R. Agency, *Gadolinium-containing contrast agents: removal of Omniscan and iv Magnevist, restrictions to the use of other linear agents*, 2017.
- 70 L. G. Nielsen, A. K. R. Junker and T. J. Sørensen, Composed in the f-block: solution structure and function of kinetically inert lanthanide(III) complexes, *Dalton Trans.*, 2018, **47**(31), 10360–10376, DOI: [10.1039/C8DT01501E](https://doi.org/10.1039/C8DT01501E).
- 71 D. Esteban-Gómez, L. A. Büldt, P. Pérez-Lourido, L. Valencia, M. Seitz and C. Platas-Iglesias, Understanding the Optical and Magnetic Properties of Ytterbium(III) Complexes, *Inorg. Chem.*, 2019, **58**(6), 3732–3743, DOI: [10.1021/acs.inorgchem.8b03354](https://doi.org/10.1021/acs.inorgchem.8b03354).
- 72 M.-E. Boulon, G. Cucinotta, J. Luzon, C. Degl'Innocenti, M. Perfetti, K. Bernot, G. Calvez, A. Caneschi and R. Sessoli, Magnetic Anisotropy and Spin-Parity Effect Along the Series of Lanthanide Complexes with DOTA, *Angew. Chem., Int. Ed.*, 2013, **52**(1), 350–354, DOI: [10.1002/anie.201205938](https://doi.org/10.1002/anie.201205938).
- 73 C. A. P. Goodwin, D. Reta, F. Ortu, N. F. Chilton and D. P. Mills, Synthesis and Electronic Structures of Heavy Lanthanide Metallocenium Cations, *J. Am. Chem. Soc.*, 2017, **139**(51), 18714–18724, DOI: [10.1021/jacs.7b11535](https://doi.org/10.1021/jacs.7b11535).
- 74 D. Errulat, R. Marin, D. A. Gálico, K. L. M. Harriman, A. Pialat, B. Gabidullin, F. Iikawa, O. D. D. Couto Jr., J. O. Moilanen, E. Hemmer, *et al.*, A Luminescent Thermometer Exhibiting Slow Relaxation of the Magnetization: Toward Self-Monitored Building Blocks for Next-Generation Optomagnetic Devices, *ACS Cent. Sci.*, 2019, **5**(7), 1187–1198, DOI: [10.1021/acscentsci.9b00288](https://doi.org/10.1021/acscentsci.9b00288).

- 75 G. Cucinotta, M. Perfetti, J. Luzon, M. Etienne, P.-E. Car, A. Caneschi, G. Calvez, K. Bernot and R. Sessoli, Magnetic Anisotropy in a Dysprosium/DOTA Single-Molecule Magnet: Beyond Simple Magneto-Structural Correlations, *Angew. Chem., Int. Ed.*, 2012, **51**(7), 1606–1610, DOI: [10.1002/anie.201107453](https://doi.org/10.1002/anie.201107453).
- 76 A. A. Kitos, D. A. Gállico, N. Mavragani, R. Castañeda, J. O. Moilanen, J. L. Brusso and M. Murugesu, Probing optical and magnetic properties via subtle stereoelectronic effects in mononuclear DyIII-complexes, *Chem. Commun.*, 2021, **57**(63), 7818–7821, DOI: [10.1039/D1CC02407H](https://doi.org/10.1039/D1CC02407H).
- 77 F. Pointillart, O. Cador, B. Le Guennic and L. Ouahab, Uncommon lanthanide ions in purely 4f Single Molecule Magnets, *Coord. Chem. Rev.*, 2017, **346**, 150–175, DOI: [10.1016/j.ccr.2016.12.017](https://doi.org/10.1016/j.ccr.2016.12.017).
- 78 F. Gendron, S. Di Pietro, L. Abad Galán, F. Riobé, V. Placide, L. Guy, F. Zinna, L. Di Bari, A. Bensalah-Ledoux, Y. Guyot, *et al.*, Luminescence, chiroptical, magnetic and ab initio crystal-field characterizations of an enantiopure helicoidal Yb(iii) complex, *Inorg. Chem. Front.*, 2021, **8**(4), 914–926, DOI: [10.1039/D0QI01194K](https://doi.org/10.1039/D0QI01194K).